Supporting Information†

A novel microporous hydrogen-bonded framework with electron-rich alkynyl groups for highly efficient C_2H_6/C_2H_4 separation

Yu-Bo Wang[a], Teng-Fei Zhang[a], Yu-Xin Lin[a], Jia-Xin Wang[a], Hui-Min Wen[b], Xu Zhang*[c], Guodong Qian[a] and Bin Li*[a]

[a] State Key Laboratory of Silicon and Advanced Semiconductor Materials, School of Materials Science and Engineering, Zhejiang University, Hangzhou 310027, China

E-mail: bin.li@zju.edu.cn

[b] College of Chemical Engineering, Zhejiang University of Technology Hangzhou 310014, China

[c] Jiangsu Engineering Laboratory for Environmental Functional Materials School of Chemistry and Chemical Engineering, Huaiyin Normal University, Huaian 223300, China

E-mail: zhangxu@hytc.edu.cn

Table of Contents

Supplementary Experimental Section

1. Fitting of pure component isotherms

The experimentally measured loadings for C_2H_6 and C_2H_4 measured at temperatures of 296 K, ZJU-HOF-60a were fitted with the dual-Langmuir-Freundlich isotherm model:

$$q = q_{A,sat}\frac{b_A p^{\nu_A}}{1+b_A p^{\nu_A}} + q_{B,sat}\frac{b_B p^{\nu_B}}{1+b_B p^{\nu_B}} \quad (1)$$

with T-dependent parameters b_A, and b_B

$$b_A = b_{A0}\exp\left(\frac{E_A}{RT}\right); b_B = b_{B0}\left(\frac{E_B}{RT}\right) \quad (2)$$

The parameters are provided in Table S3.

2. Virial Graph Analysis

Estimation of isosteric heats of gas adsorption (Q_{st})

A virial-type expression comprising the temperature-independent parameters a_i and b_j was employed to calculate the enthalpies of adsorption for C_2H_6 and C_2H_4 (at 273 K, 296 K, and 313 K) on ZJU-HOF-60a. In each case, the data were fitted using the equation:

$$\ln P = \ln N + 1/T\sum_{i=1}^{m} a_i N_i + \sum_{j=1}^{n} b_j N_j \quad (3)$$

Here, P is the pressure expressed in mmHg, N is the amount absorbed in mmol g^{-1}, T is the temperature in K, a_i and b_j are virial coefficients, and m, n represent the number of coefficients required to adequately describe the isotherms (m and n were gradually increased till the contribution of extra added a and b coefficients was deemed to be statistically insignificant towards the overall fit. And the average value of the squared deviations from the experimental values was minimized). The values of the virial coefficients a_0 through a_m were then used to calculate the isosteric heat of absorption using the following expression:

$$Q_{st} = -R\sum_{i=0}^{m} a_i N_i \quad (4)$$

Q_{st} is the coverage-dependent isosteric heat of adsorption and R is the universal gas

constant. The heat enthalpy of C_2H_6 and C_2H_4 sorption for ZJU-HOF-60a in this manuscript are determined by using the sorption data measured in the pressure range from 0–1 bar (at 273 K, 296 K, and 313 K).

3. IAST calculations

The selectivity of preferential adsorption of component 1 (C_2H_6) over component 2 (C_2H_4) can be defined as the following equation:

$$S_{ads} = \frac{q_1/q_2}{p_1/p_2} \tag{5}$$

In equation (5), q_1 and q_2 are the molar loadings in the adsorbed phase in equilibrium with the bulk gas phase with partial pressures p_1, and p_2. The component loadings and adsorption selectivity S_{ads} for 50/50 C_2H_6 (1)/C_2H_4 (2) and 10/90 C_2H_6 (1)/C_2H_4 (2) mixtures in ZJU-HOF-60a at 296 K were determined using IAST.

4. Density functional theory (DFT) calculations

The structure of ZJU-HOF-60a was optimized in the Dmol^3 module, using the generalized gradient approximation (GGA) with the Perdew-Burke-Ernzerhof (PBE) functional and the double numerical plus d-functions (DNP) basis set.[1–3] The energy, force, and displacement convergence criteria were set as 1×10^{-5} Ha, 2×10^{-3} Ha/Å and 5×10^{-3} Å, respectively. Single point energy calculations with the same parameters using Dmol^3 were performed on the optimized ZJU-HOF-60a structure. The electron density data obtained from these calculations were used to construct the 0.15 e^- Å^{-3} electron density isosurfaces of the framework, with a grid interval of 0.1 Å. The calculated electrostatic potential for ZJU-HOF-60a was then mapped onto their electron density isosurfaces.

5. Quantification of the diffusion rate

The diffusion rate was measured on a BELSORP-max II (BEL Japan, Inc.) automated volumetric sorption analyzer and was fitted automatically with BEL-Master software according

to the Crank theory described in the reported literatures.[4–6]

Adsorption rate equation in consideration of in-particle diffusion (assuming spherical particle):

$$\frac{\partial q}{\partial t} = D_s\left(\frac{\partial^2 q}{\partial r^2} + \frac{2}{r} \times \frac{\partial q}{\partial r}\right) \tag{6}$$

Boundary condition: When $r = R,\ q = q_{0n}$

Linear equilibrium equation: $q^* = H \times P$ (7)

Here, H is equilibrium constant in $m^3\ g^{-1}$, p is pressure in Pa.

Equation (8) for batch adsorbing operation is used.

$$W(q - q_{0n}) = V(p_{0n} - p) \tag{8}$$

W is mass of adsorbent (g), V is fluid volume (m^3).

By solving simultaneous equations of the above (6), (7), and (8), the following solution is obtained:

$$\frac{p}{p_{0n}} = 1 - \left(\frac{1}{\alpha + 1}\right)\left[1 - \Sigma_{n=1}^{\infty} \frac{6\alpha(\alpha + 1)\exp(-q_n^2 \tau_s)}{9 + 9\alpha + q_n^2 \alpha^2}\right] \tag{9}$$

Equation (9) is called “Crank equation”.

$$\frac{p - p_{en}}{p_{0n} - p_{en}} = 1 - \left(\frac{p_{0n} - p_{en-1}}{p_{0n} - p_{en}}\right)\left(\frac{1}{\alpha + 1}\right)\left[1 - \Sigma_{n=1}^{\infty} \frac{6\alpha(\alpha + 1)\exp(-q_n^2 \tau_s)}{9 + 9\alpha + q_n^2 \alpha^2}\right] \tag{10}$$

With gas state Equation ($p = cRT$), Equation (10) is expressed as the following equation, from which solution of analysis considering pore diffusion can be obtained.

$$\frac{C - C_{en}}{C_{0n} - C_{en}} = 1 - \left(\frac{C_{0n} - c_{en-1}}{C_{0n} - C_{en}}\right)\left(\frac{1}{\alpha + 1}\right)\left[1 - \Sigma_{n=1}^{\infty} \frac{6\alpha(\alpha + 1)\exp(-q_n^2 \tau_s)}{9 + 9\alpha + q_n^2 \alpha^2}\right] \tag{11}$$

Wherein, $\tau_s = \frac{D_s}{R^2} t$, $\alpha = \frac{V}{W \times H}$

For the adsorption rate analysis program, equation (11) is used.

6. Grand canonical Monte Carlo simulations

To obtain the reasonable binding sites of gas molecules in ZJU-HOF-60a for subsequent modeling, grand canonical Monte Carlo (GCMC) simulations were performed. The crystal structures of ZJU-HOF-60a were chosen for related simulations without further geometry optimization. The framework and the individual C_2H_6 and C_2H_4 molecules were considered to be rigid during the simulation. Partial charges for atoms of guest-free ZJU-HOF-60a were derived from QEq method and QEq_neutral1.0 parameter. The simulations were carried out at 298 K, adopting the locate task, Metropolis method in the Sorption module and the universal force field (UFF). The partial charges on the atoms of C_2H_6 (C: −0.455e; H: 0.152e, where e = 1.6022×10^{-19} C is the elementary charge) and C_2H_4 (C: −0.293e; H: 0.147e) were also derived from QEq method. The interaction energy between hydrocarbon molecules and framework was computed through the Coulomb and Lennard-Jones 6-12 Lennard-Jones (LJ) potentials. The cutoff radius was chosen as 15.5 Å for the LJ potential and the long-range electrostatic interactions were handled using the Ewald & Group summation method. The loading steps and the equilibration steps were 1×10^5, the production steps were 1×10^6.

7. Gas equilibrium adsorption capacity

The complete breakthrough of C_2H_6 was indicated by the downstream gas composition reaching that of the feed gas. Based on the mass balance, the gas adsorption capacities can be determined as follows:

$$q_i = \frac{C_i V}{22.4 \times m} \times \int_0^t \left(1 - \frac{F}{F_0}\right) dt \tag{12}$$

where q_i is the equilibrium adsorption capacity of gas i (mmol g^{-1}), C_i is the feed gas concentration, V is the volumetric feed flow rate (cm^3 min^{-1}), t is the adsorption time (min), F_0 and F are the inlet and outlet gas molar flow rates, respectively, and m is the mass of the adsorbent (g).

Notation

q	component molar loading of species i, mol kg^{-1}
q_{sat}	saturation loading, mol kg^{-1}
b	Langmuir-Freundlich constant, Pa$^{-v_{iA}}$
T	absolute temperature, K
a_i	Virial coefficients, dimensionless
b_j	Virial coefficients, dimensionless
Q_{st}	isosteric heat of adsorption, kJ mol^{-1}
p_i	total system pressure, Pa
c_i	molar concentration of species i in gas mixture, mol m^{-3}
D_s	surface diffusion coefficient, cm^2 s^{-1}
H	equilibrium constant, cm^3 g^{-1}
P_0	initial pressure, Pa
P_e	equilibrium pressure, Pa
R	radius of particle, cm
t	time, s
V	Gas phase volume, cm^3
W	adsorbent amount, g

Greek letters

v	Freundlich exponent, dimensionless

Supplementary Tables

Table S1. Physicochemical properties of C_2H_6 and C_2H_4 molecules.

	Kinetic Diameter (Å)	Molecular dimensions (Å)	Boiling point (K)	Polarizability ($\times 10^{-25}$ cm^3)	Quadrupole moment ($\times 10^{-26}$ esu cm^2)
C_2H_4	4.16	3.28 × 4.18 × 4.84	169.5	42.52	1.50
C_2H_6	4.44	3.81 × 4.82 × 4.08	184.6	44.70	0.65

Table S2. Crystallographic data and structure refinement results of ZJU-HOF-60 and ZJU-HOF-60a.

	ZJU-HOF-60	ZJU-HOF-60a
Formula	$C_{18}H_{10}O_8$	$C_{18}H_{10}O_8$
Formula weight	354.26	354.26
Crystal system	triclinic	monoclinic
Space group	$P\bar{1}$	$I2/m$
a (Å)	6.824(2)	3.647(3)
b (Å)	14.235(4)	16.438(14)
c (Å)	14.278(3)	20.954(2)
α (°)	70.00(3)	90
β (°)	88.62(2)	91.58(6)
γ (°)	76.31(2)	90
Cell volume (Å^3)	1263.83(6)	1255.47(19)
Z	2	2
D_{calc} (g·cm^{-3})	0.930864	0.937063
μ (mm^{-1})	0.642	0.646
$F(000)$	364	364
GOF	0.961	1.043
R_{int}	0.1904	0.0560
R_1, wR_2 [I>=2σ (I)]	0.0768, 0.1997	0.0697, 0.1915
R_1, wR_2 [all data]	0.1400, 0.2451	0.0734, 0.1957
Largest diff. peak and hole	0.329 and -0.324	0.482 and -0.248

CCDC number	2358377	2358378

Table S3. Dual-site Langmuir-Freundlich parameter fits for C_2H_6 and C_2H_4 in ZJU-HOF-60a. The fits are based on experimental isotherm data at 296 K.

	Site A			Site B		
	$q_{A,sat}$	b_{A0}	v_A	$q_{B,sat}$	b_{B0}	v_B
	mol kg^{-1}	kPa$^{-v_A}$	dimensionless	mol kg^{-1}	kPa$^{-v_B}$	dimensionless
C_2H_6	2.73416	0.01517	0.93680	5.26969	4.5747×10^{-4}	1.62180
C_2H_4	3.30884	0.00641	1.05327	2.13327	3.0779×10^{-5}	2.19194

Table S4. Summary of separation metrics of C_2H_6-selective HOF materials reported in the literature at 1 bar and room temperature (RT).

	C_2H_6 uptake[a] (mmol g^{-1})	C_2H_6/C_2H_4 uptake ratio[b]	IAST selectivity[c]	Productivity[d] (L kg^{-1})	Ref.
HOF-BTB[e]	3.09	1.24	1.4	−	7
HOF-76a	2.95	1.77	2.0	7.2	8
ZJU-HOF-1	4.87	1.22	2.25	21.9	9
ZJU-HOF-10(sc)	2.19	1.17	1.9	6.9	10
HOF-NBDA	3.98	1.36	1.75	−	1
MTHOF-1	1.27	1.09	2.15	−	11
HIAM-102	2.15	1.09	1.9	5.3	12
HIAM-103	1.56	1.04	1.6	4.4	13
ZJU-HOF-60a	**3.79**	**1.58**	**1.8**	**7.8**	**This work**

[a] C_2H_6 uptake at 1 bar and RT.

[b] C_2H_6/C_2H_4 uptake ratio at 1 bar and RT.

[c] IAST selectivity for 50/50 C_2H_6/C_2H_4 gas mixtures.

[d] The pure C_2H_4 productivity calculated from breakthrough experiments at 1 bar and RT on 50/50 gas mixtures.

[e] The reported literature only described the C_2H_4 and C_2H_6 adsorption isotherms, so the selectivity was evaluated based on these isotherms.

Supplementary Figures

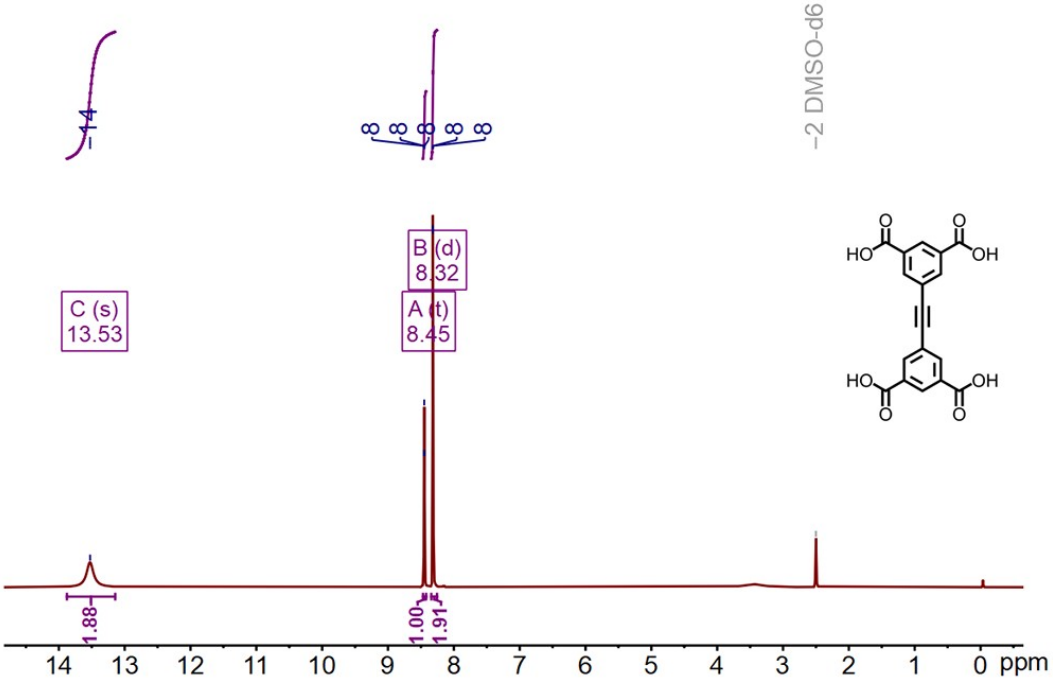

Figure S1. ^{1}H NMR spectrum of H_4EBDC in DMSO-d_6.

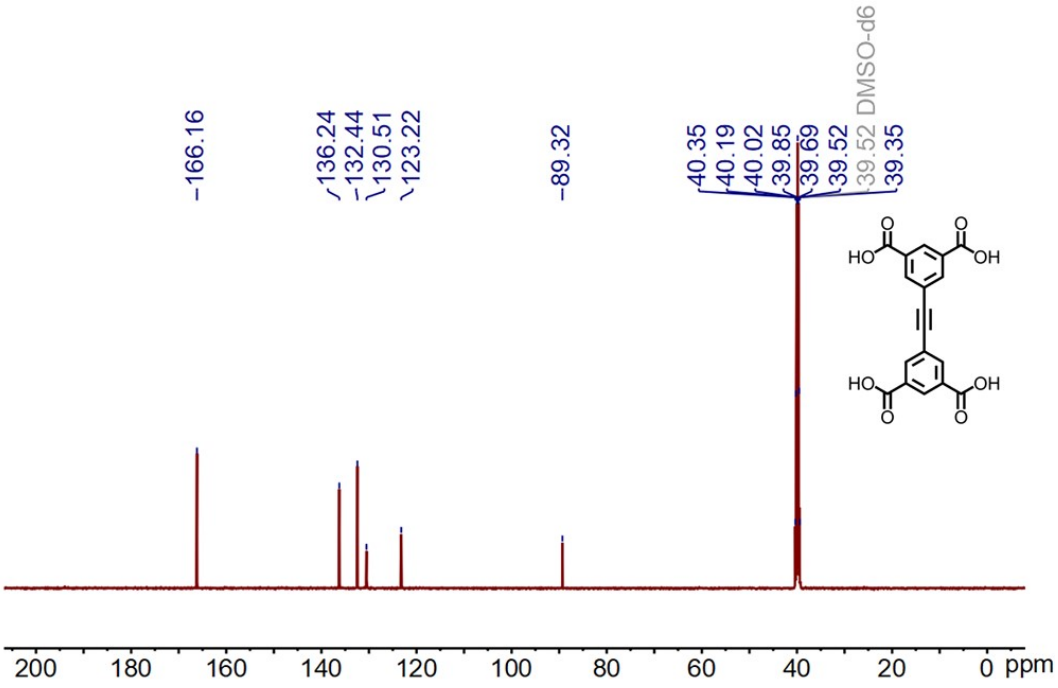

Figure S2. ^{13}C NMR spectrum of H_4EBDC in DMSO-d_6.

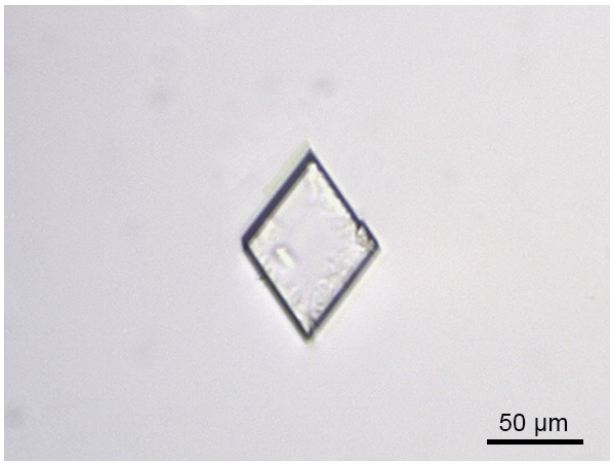

Figure S3. The optical photos of the as-synthesized crystal of ZJU-HOF-60.

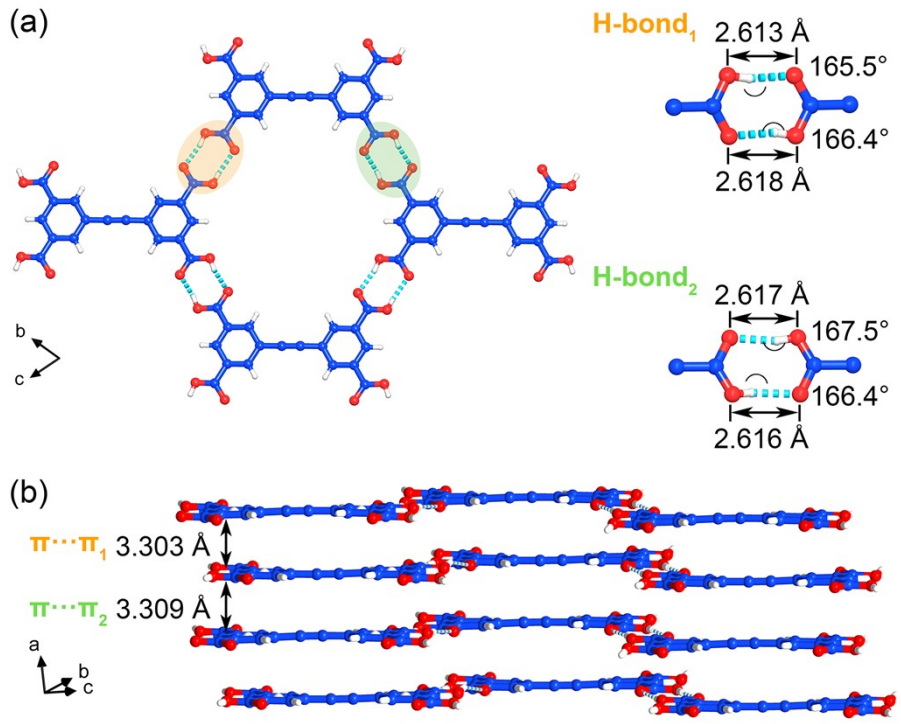

Figure S4. Crystal structure description of ZJU-HOF-60 (C, blue; O, red; H, white). (a) Illustration of the hydrogen bond connection in ZJU-HOF-60. The H_4EBDC molecule is connected to the surrounding molecules by two different sets of carboxyl···carboxyl dimer linkage with the O–H···O distance from 2.613 to 2.618 Å, and the angles varying from 165.5° to 167.5°. (b) The layered frameworks of ZJU-HOF-60 are arranged in a staggered AA stacking pattern, with the π···π stacking interactions (average distance of 3.306 Å) from the phenyl rings and the C≡C.

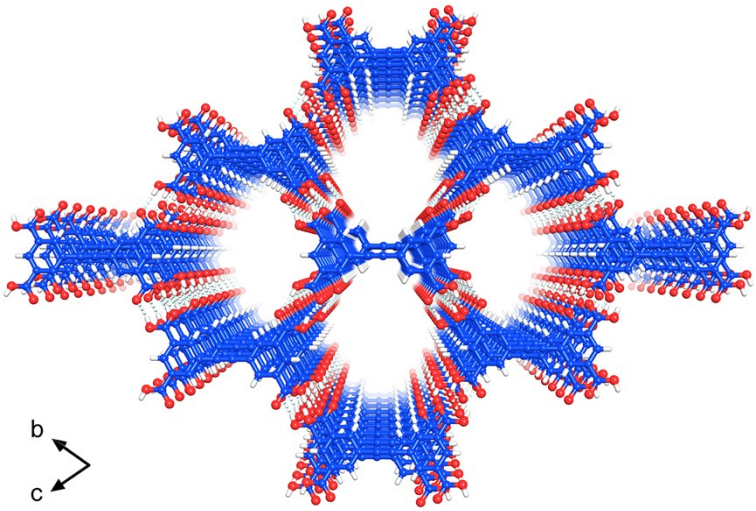

Figure S5. The framework structure of ZJU-HOF-60. Color code: C (blue), O (red), and H (white).

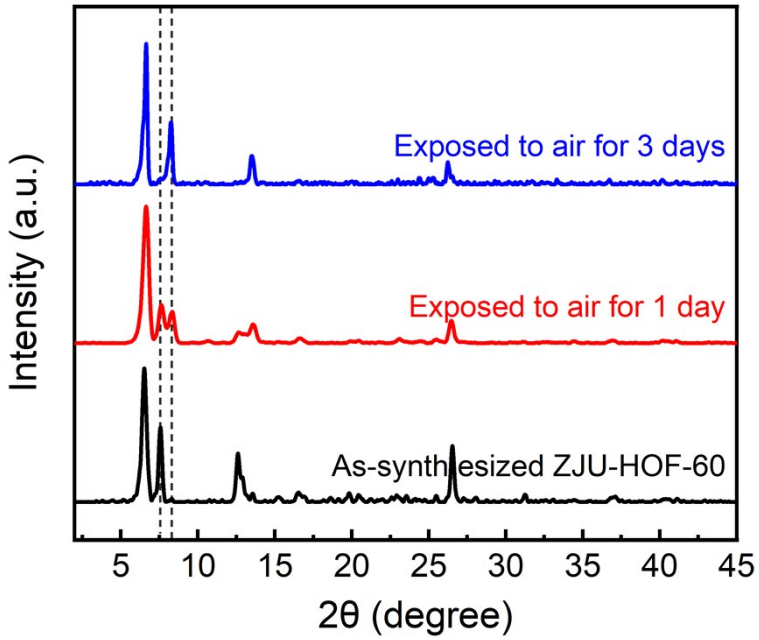

Figure S6. PXRD patterns of as-synthesized samples ZJU-HOF-60 exposed to air for 3 days, indicating that ZJU-HOF-60 can transform into the activated ZJU-HOF-60a after the guest solvents evaporate away.

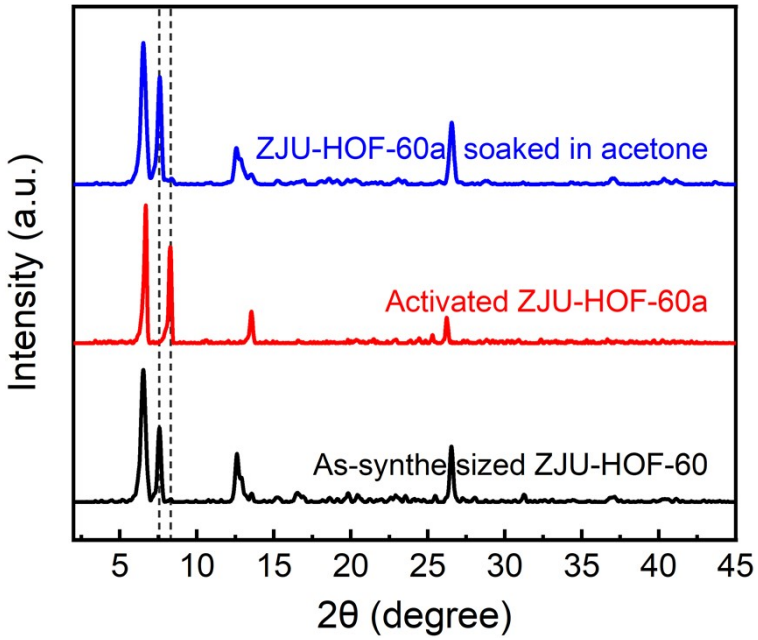

Figure S7. PXRD patterns for activated ZJU-HOF-60a after soaking in acetone, indicate that the framework of ZJU-HOF-60a can reversibly transform into ZJU-HOF-60.

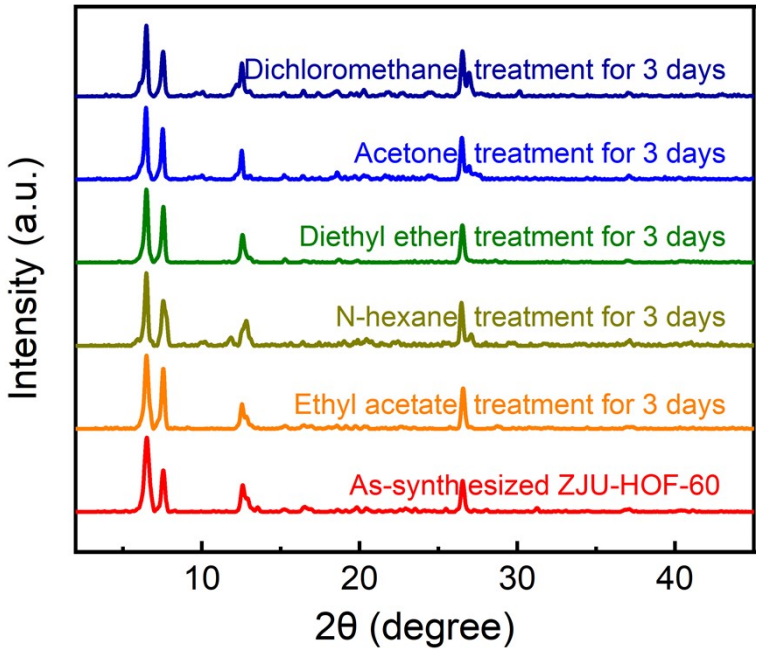

Figure S8. PXRD patterns for as-synthesized ZJU-HOF-60 after soaking in various organic solvents.

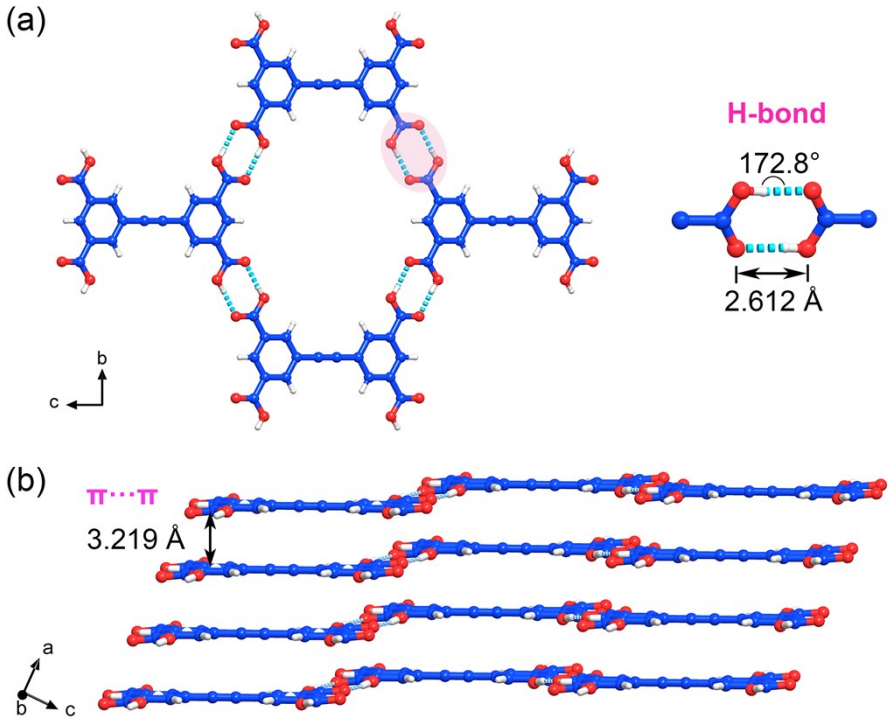

Figure S9. Crystal structure description of ZJU-HOF-60a (C, blue; O, red; H, white). (a) Illustration of the hydrogen bond connection in ZJU-HOF-60a. The H_4EBDC molecules are arranged by the carboxyl dimer, and the O–H···O distance and angle are 2.612 Å and 172.8°, respectively. (b) The 2D layers of ZJU-HOF-60a are stacked in an eclipsed AA stacking pattern with π···π interactions (distance of 3.219 Å).

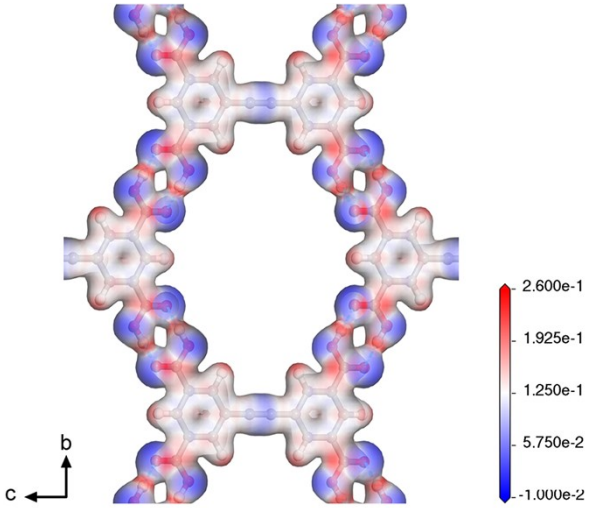

Figure S10. The ESP of pore channels for ZJU-HOF-60a. (viewed along the *a*-axis). The gradation on the scale bar is in Hartree/e.

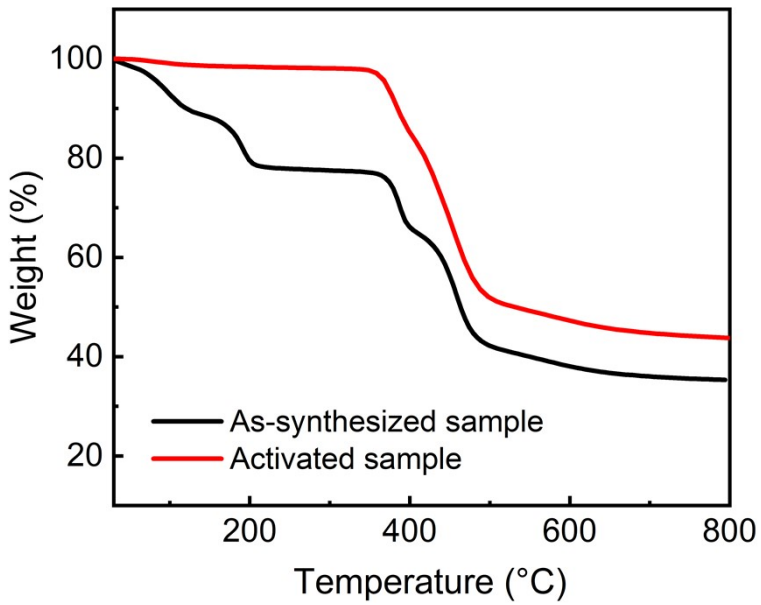

Figure S11. TGA curve of the as-synthesized sample ZJU-HOF-60 (black) and the activated ZJU-HOF-60a (red).

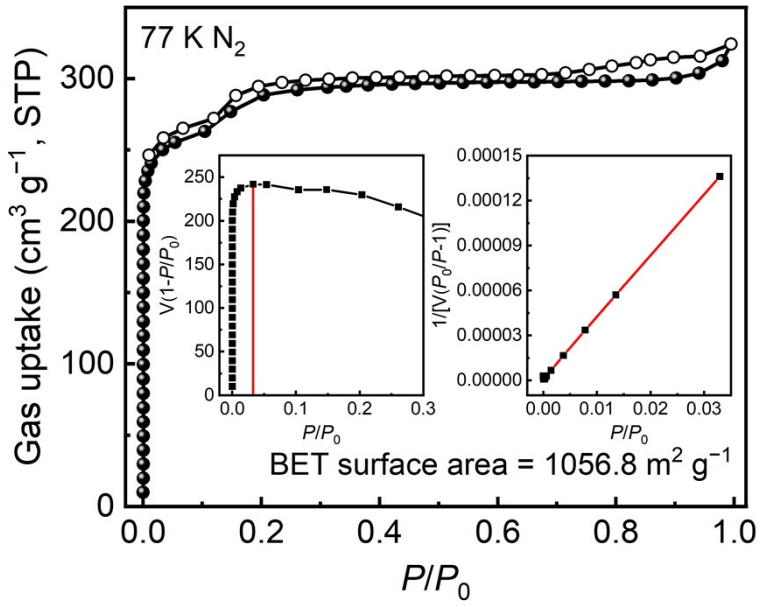

Figure S12. Nitrogen adsorption isotherm at 77 K with consistency and BET plots for the activated ZJU-HOF-60a sample.

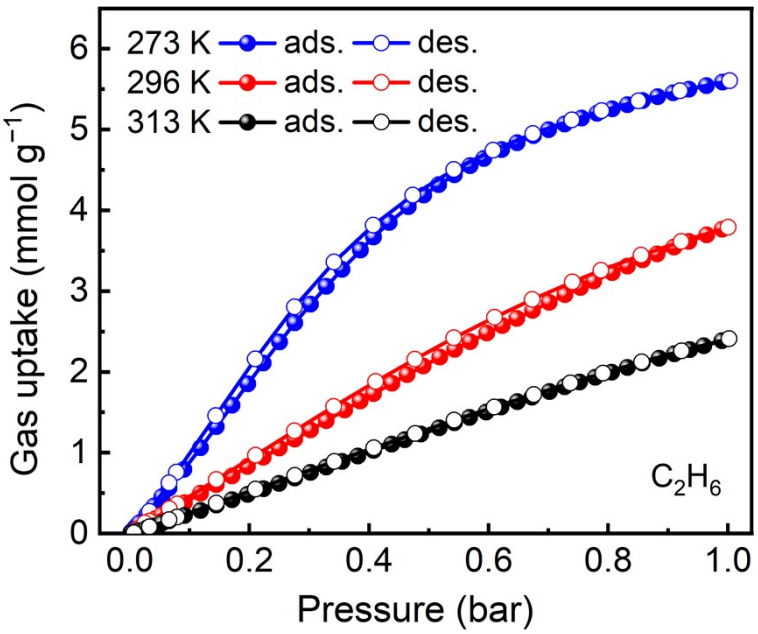

Figure S13. Adsorption isotherms of C_2H_6 for ZJU-HOF-60a at 273 (blue), 296 K (red), and 313 K (black) up to 1 bar. Filled/empty symbols represent adsorption/desorption.

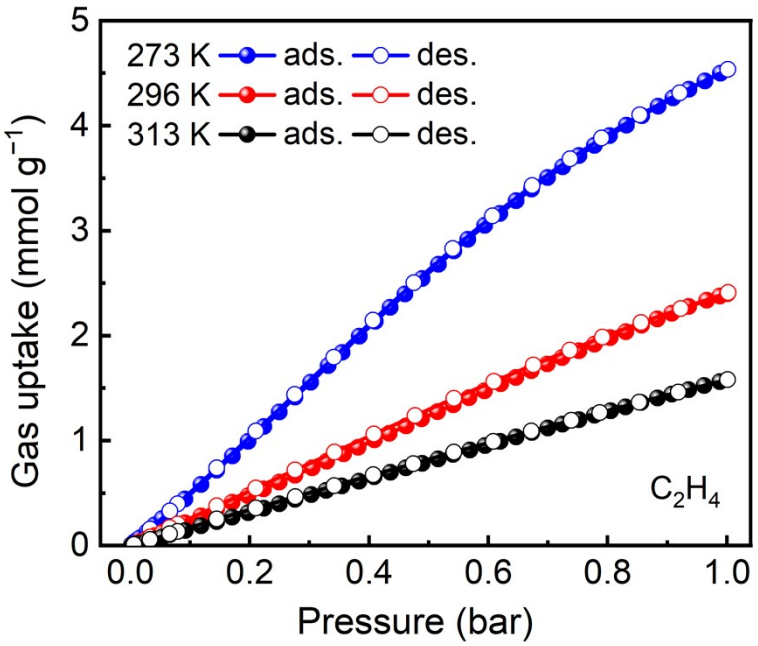

Figure S14. Adsorption isotherms of C_2H_4 for ZJU-HOF-60a at 273 (blue), 296 K (red), and 313 K (black) up to 1 bar. Filled/empty symbols represent adsorption/desorption.

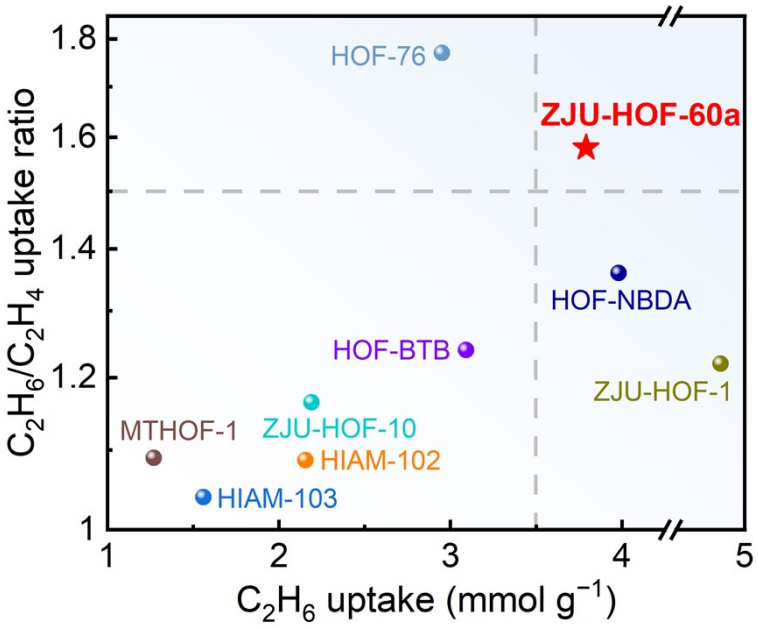

Figure S15. Comparison of C_2H_6 uptake capacity and C_2H_6/C_2H_4 uptake ratio at 1 bar and room temperature for ZJU-HOF-60a and other reported C_2H_6-selective HOF materials.

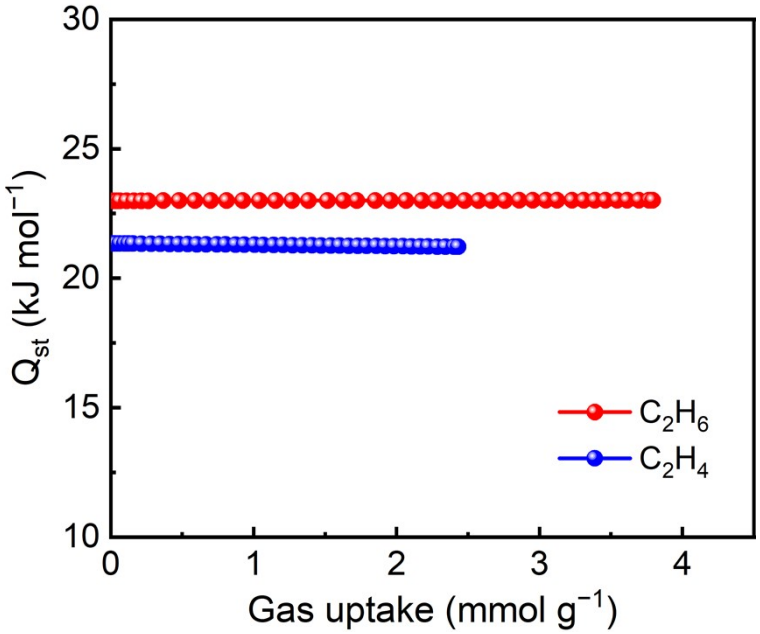

Figure S16. Adsorption heat of the C_2H_6 (red) and C_2H_4 (blue) for ZJU-HOF-60a.

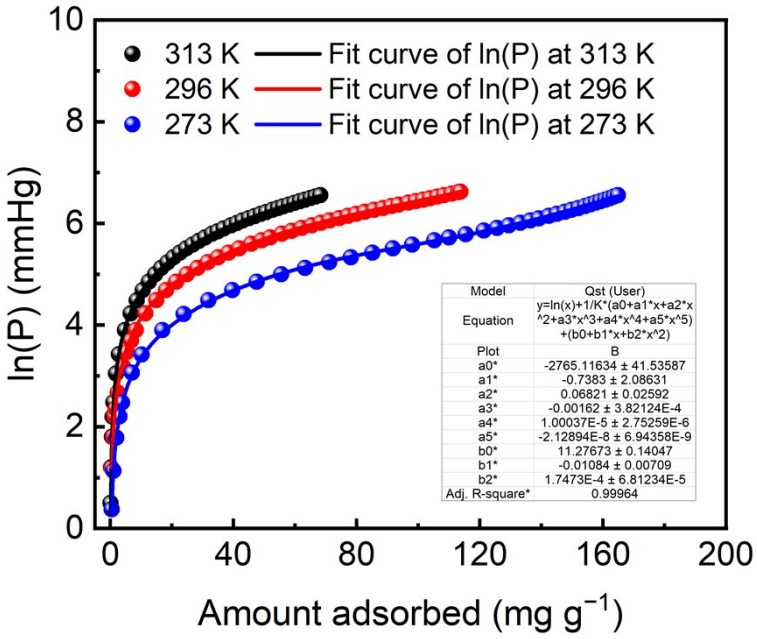

Figure S17. Virial fitting of the C_2H_6 adsorption isotherms for ZJU-HOF-60a.

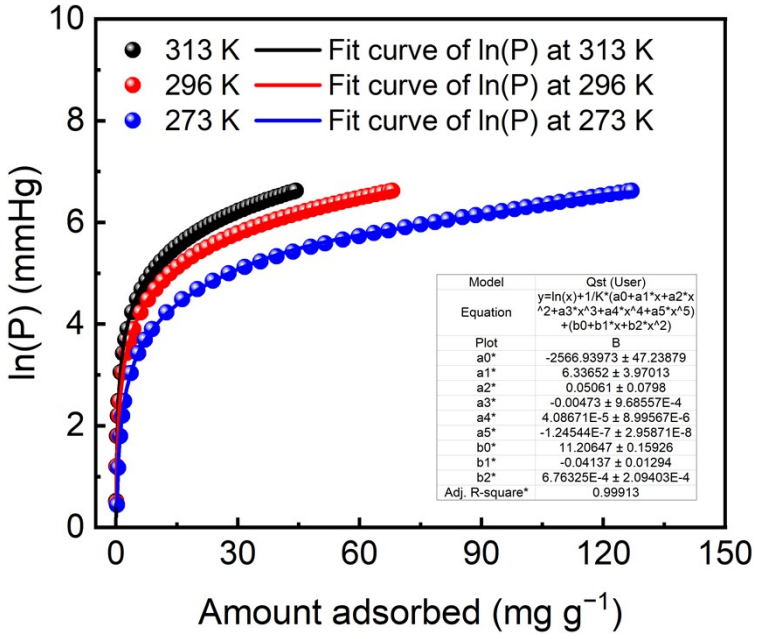

Figure S18. Virial fitting of the C_2H_4 adsorption isotherms for ZJU-HOF-60a.

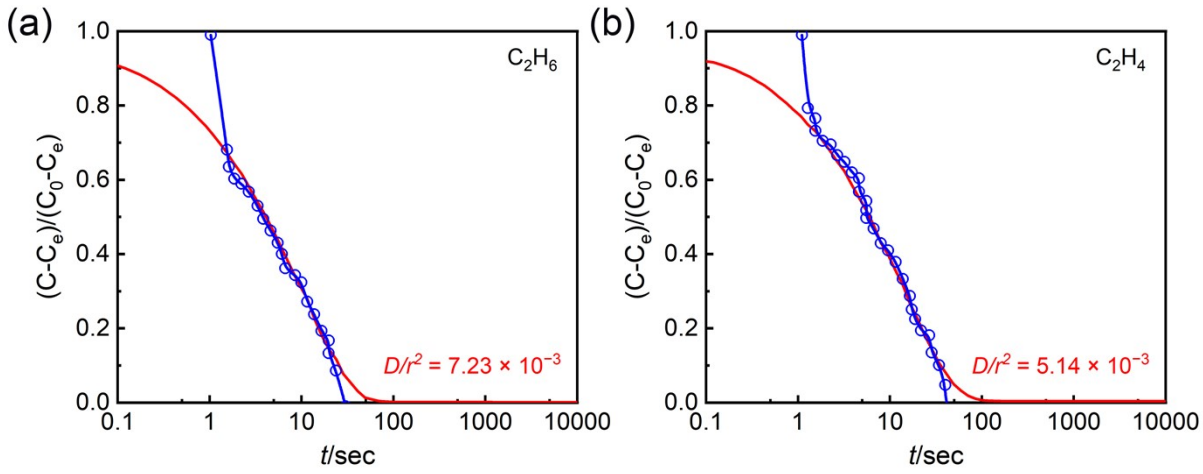

Figure S19. The calculated (a) C_2H_6 and (b) C_2H_4 diffusion rate constants on ZJU-HOF-60, fitted automatically with BEL-Master software according to the Crank theory. *C*, concentration; C_0, initial concentration; C_e, concentration at equilibrium.

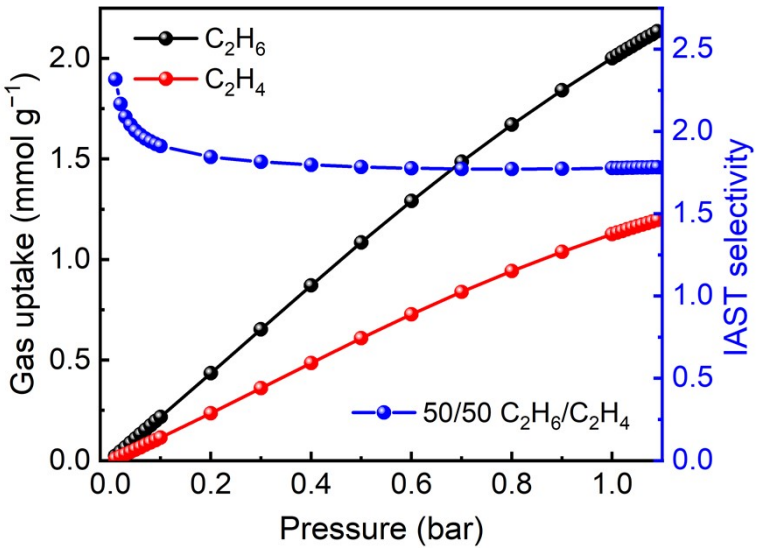

Figure S20. Predicted mixture adsorption isotherms (left *Y*-axis) and selectivity (right *Y*-axis) of ZJU-HOF-60a predicted by the IAST method for a 50/50 (v/v) C_2H_6/ C_2H_4 mixture at 296 K.

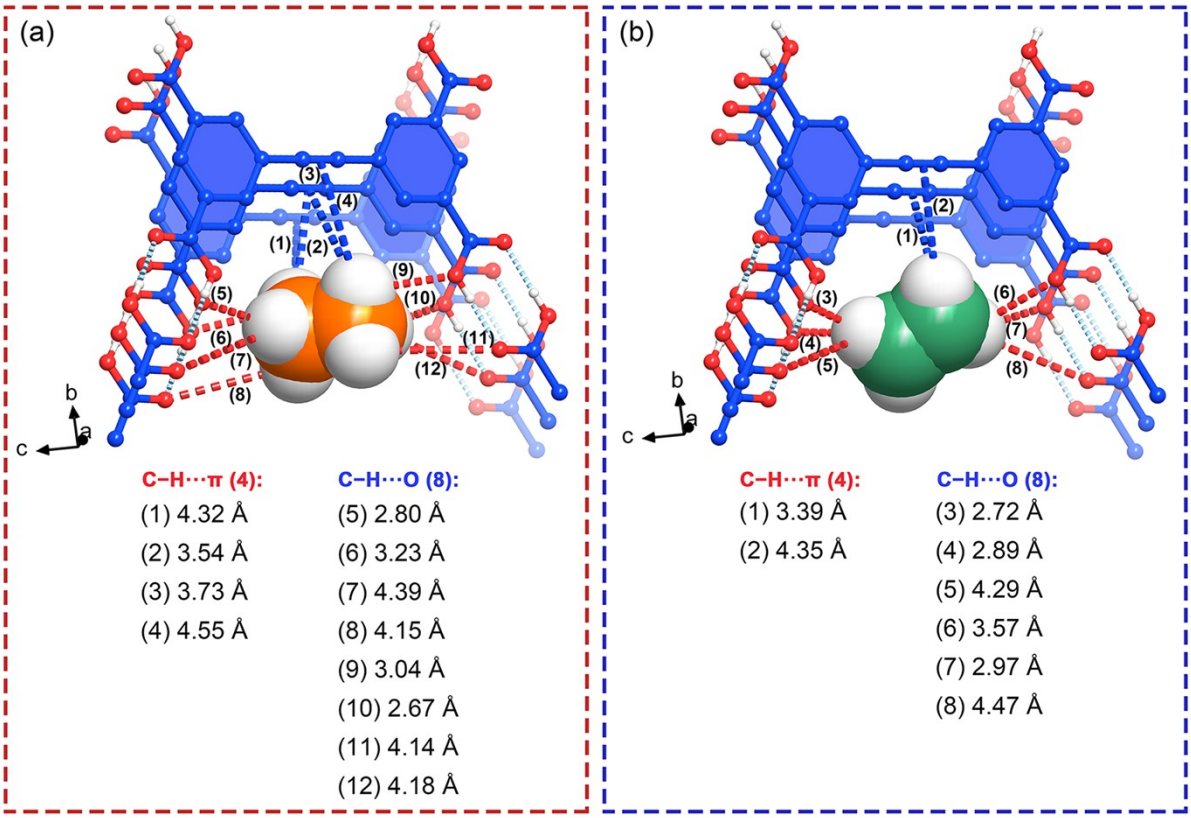

Figure S21. Comparison of the preferential C_2H_6 and C_2H_4 adsorption sites and the close van der Waals contacts within the rhombic pores in ZJU-HOF-60a (C, blue; O, red; H, white) observed by GCMC simulations, highlighting the C−H···π interactions (blue dashed lines) and C−H···O (red dashed lines) interactions. The hydrogen atoms in the benzene ring are omitted for clarity.

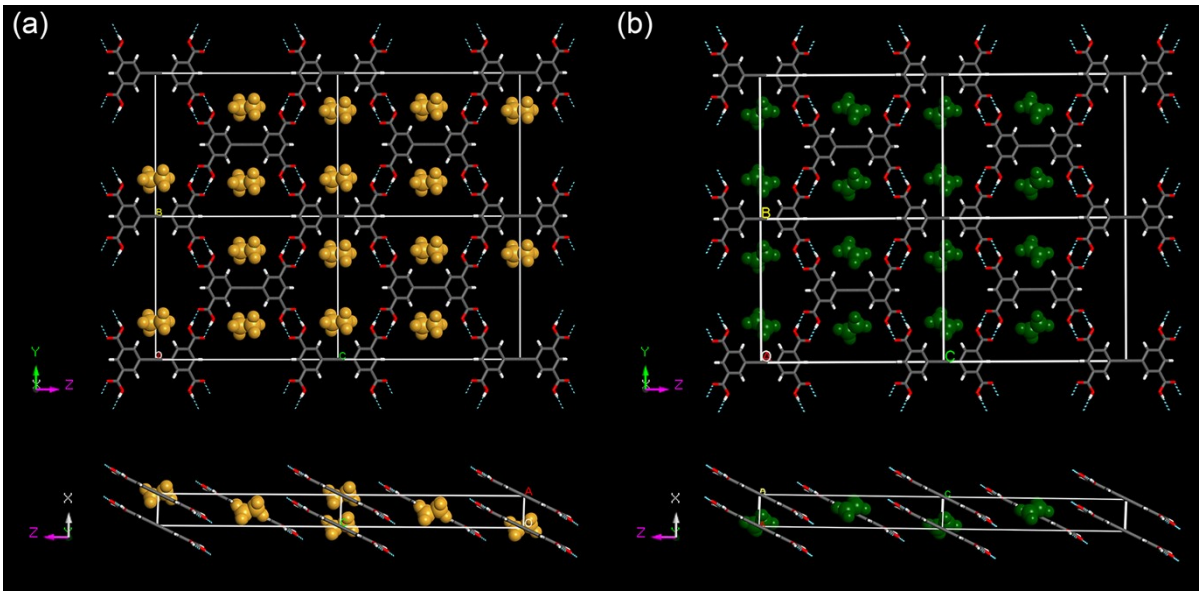

Figure S22. A local structure of ZJU-HOF-60a showing all the adsorbed gas molecules for (a) C_2H_6 and (b) C_2H_4. There exist four gas molecules within each unit cell if all the binding sites are fully occupied.

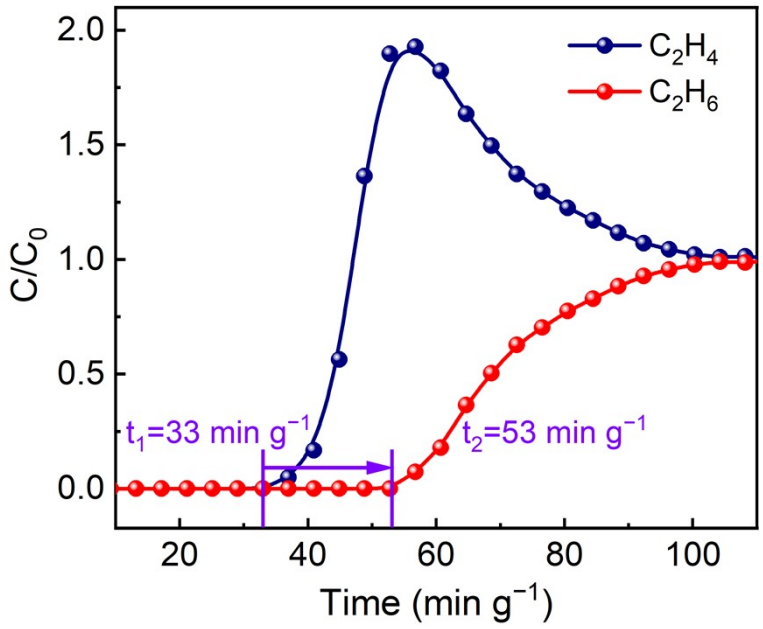

Figure S23. The calculation of the C_2H_4 productivity during the breakthrough process of 50/50 C_2H_6/C_2H_4 mixtures in ZJU-HOF-60a. The flow rate of C_2H_4 is 1.25 mL/min and the sample weight is 0.758 g. The C_2H_4 productivity is defined by the breakthrough amount of C_2H_4, which is calculated by integration of the breakthrough curves *f(t)* during a period from t_1 (33 min g^{-1}) to t_2 (53 min g^{-1}) where the C_2H_4 purity is higher than or equal to the threshold value of 99.95%. The C_2H_4 productivity is calculated to be 7.8 L kg^{-1} based on equation (12).

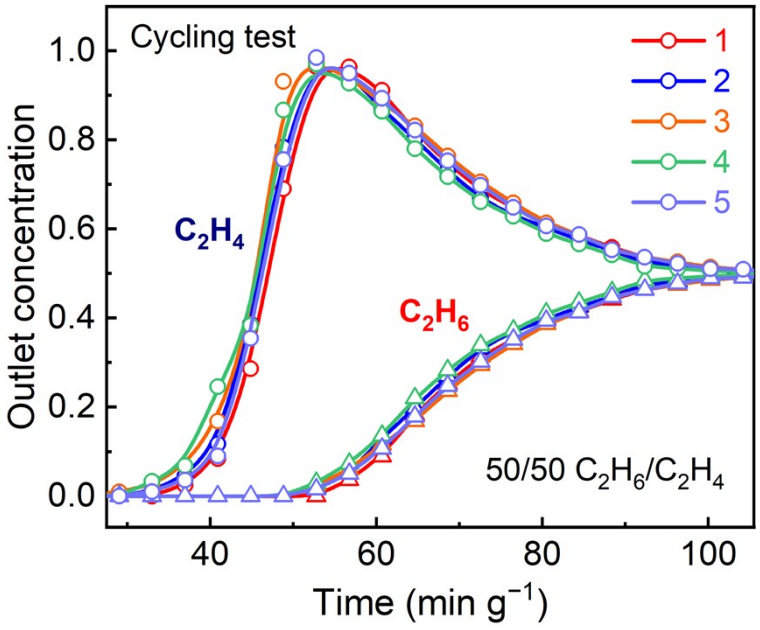

Figure S24. Cyclic breakthrough experiments for C_2H_6/C_2H_4 (50/50, v/v) separation of ZJU-HOF-60a at room temperature.

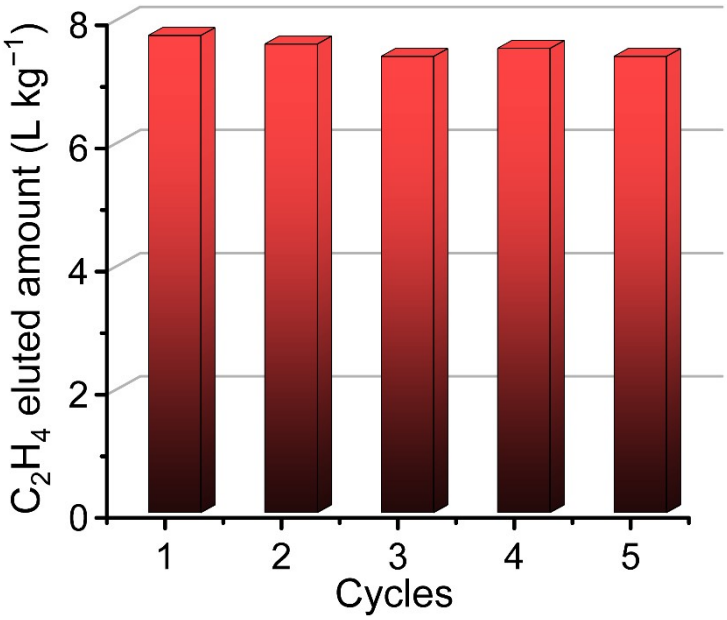

Figure S25. The high-purity C_2H_4 productivity of cyclic breakthrough experiments for C_2H_6/C_2H_4 (50/50) mixture on ZJU-HOF-60a at room temperature, indicating that there was no obvious loss in the elution amount of high-purity C_2H_4 within five continuous cycles.

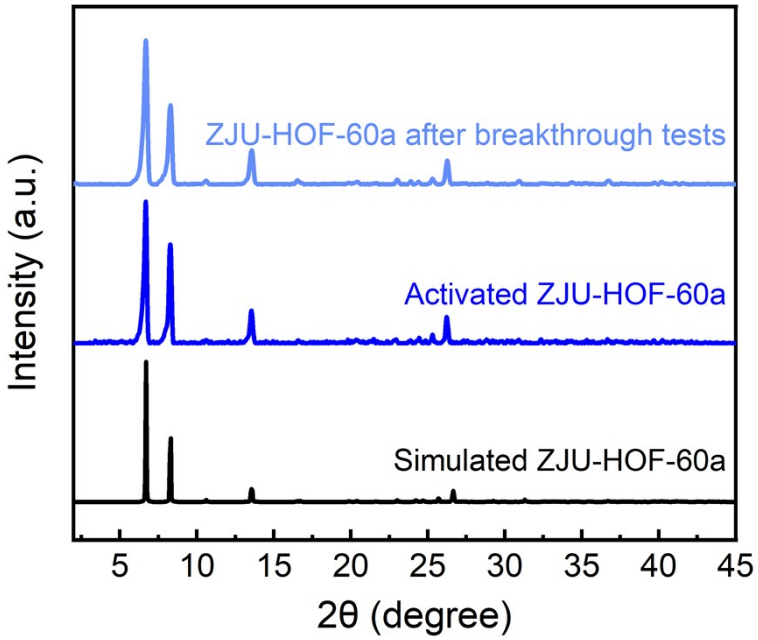

Figure S26. PXRD patterns for ZJU-HOF-60a after the test, indicate that ZJU-HOF-60a maintains structural integrity after multiple adsorption tests and breakthrough experiments.

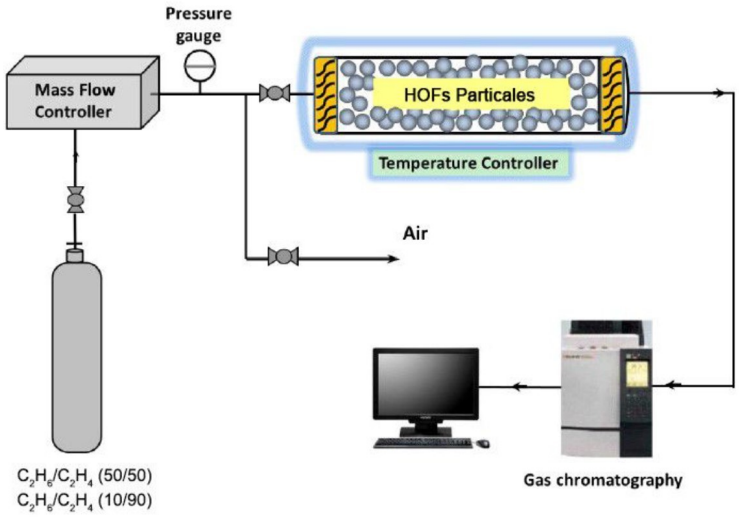

Breakthrough experiments apparatus

Figure S27. Schematic illustration of the apparatus for the breakthrough experiments.

Supplementary References

[1] Y. Zhou, C. Chen, R. Krishna, Z. Ji, D. Yuan and M. Wu, *Angew. Chem. Int. Ed.*, 2023, **62**, e202305041.

[2] H.-M. Wen, C. Yu, M. Liu, C. Lin, B. Zhao, H. Wu, W. Zhou, B. Chen and J. Hu, *Angew. Chem. Int. Ed.*, 2023, **62**, e202309108.

[3] Y. Xie, H. Cui, H. Wu, R.-B. Lin, W. Zhou and B. Chen, *Angew. Chem. Int. Ed.*, 2021, **60**, 9604–9609.

[4] H. Zeng, M. Xie, T. Wang, R.-J. Wei, X.-J. Xie, Y. Zhao, W. Lu and D. Li, *Nature*, 2021, **595**, 542–548.

[5] L. Li, L. Guo, D. H. Olson, S. Xian, Z. Zhang, Q. Yang, K. Wu, Y. Yang, Q. Ren and J. Li, *Science*, 2022, **377**, 335–339.

[6] J. Cui, Z. Zhang, L. Yang, J. Hu, A. Jin, Z. Yang, Y. Zhao, B. Meng, Y. Zhou, J. Wang, Y. Su, J. Wang, X. Cui and H. Xing, *Science*, 2023, **383**, 179–183.

[7] T.-U. Yoon, S. B. Baek, D. Kim, E.-J. Kim, W.-G. Lee, B. K. Singh, M. S. Lah, Y.-S. Bae and K. S. Kim, *Chem. Commun.*, 2013, **54**, 9360–9363.

[8] X. Zhang, L. Li, J.-X. Wang, H.-M. Wen, R. Krishna, H. Wu, W. Zhou, Z.-N. Chen, B. Li, G. Qian and B. Chen, *J. Am. Chem. Soc.*, 2020, **142**, 633–640.

[9] X. Zhang, J.-X. Wang, L. Li, J. Pei, R. Krishna, H. Wu, W. Zhou, G. Qian, B. Chen and B. Li, *Angew. Chem. Int. Ed.*, 2021, **60**, 10304–10310.

[10] J.-X. Wang, X.-W. Gu, Y.-X. Lin, B. Li and G. Qian, *Acs Mater. Lett.*, 2021, **3**, 497–503.

[11] H. Li, C. Chen, Q. Li, X. J. Kong, Y. Liu, Z. Ji, S. Zou, M. Hong and M. Wu, *Angew. Chem. Int. Ed.*, 2024, **63**, e202401754.

[12] J. Liu, J. Miao, S. Ullah, K. Zhou, L. Yu, H. Wang, Y. Wang, T. Thonhauser and J. Li, *ACS Mater. Lett.*, 2022, **4**, 1227–1232.

[13] F.-A. Guo, K. Zhou, J. Liu, H. Wang and J. Li, *Precis. Chem.*, 2023, **1**, 524–529.